Developmental Cell *11*, 1–11, September, 2006 ©2006 Elsevier Inc. DOI 10.1016/j.devcel.2006.07.001

Cytoplasmic γ-Actin Is Not Required for Skeletal Muscle Development but Its Absence Leads to a Progressive Myopathy

Kevin J. Sonnemann,[1] Daniel P. Fitzsimons,[2] Jitandrakumar R. Patel,[2] Yewei Liu,[3] Martin F. Schneider,[3] Richard L. Moss,[2] and James M. Ervasti[1,2,4,*]

[1] Program in Cellular and Molecular Biology
[2] Department of Physiology
University of Wisconsin-Madison
Madison, Wisconsin 53706
[3] Department of Biochemistry
University of Maryland
Baltimore, Maryland 21201

Summary

Nonmuscle γ_{cyto}-actin is expressed at very low levels in skeletal muscle but uniquely localizes to costameres, the cytoskeletal networks that couple peripheral myofibrils to the sarcolemma. We generated and analyzed skeletal muscle-specific γ_{cyto}-actin knockout (*Actg1*-msKO) mice. Although muscle development proceeded normally, *Actg1*-msKO mice presented with overt muscle weakness accompanied by a progressive pattern of muscle fiber necrosis/regeneration. Functional deficits in whole-body tension and isometric twitch force were observed, consistent with defects in the connectivity between muscle fibers and/or myofibrils or at the myotendinous junctions. Surprisingly, γ_{cyto}-actin-deficient muscle did not demonstrate the fibrosis, inflammation, and membrane damage typical of several muscular dystrophies but rather presented with a novel progressive myopathy. Together, our data demonstrate an important role for minimally abundant but strategically localized γ_{cyto}-actin in adult skeletal muscle and describe a new mouse model to study the in vivo relevance of subcellular actin isoform sorting.

Introduction

Actins are a family of highly conserved cytoskeletal proteins that play fundamental roles in nearly all aspects of eukaryotic cell biology. A cell's ability to divide, move, endocytose, generate contractile force, and maintain shape is reliant upon functional actin-based structures. Therefore, efforts to identify the regulatory processes involved in actin filament function and stability are necessary to provide a deeper mechanistic understanding of the eukaryotic cell.

It is well accepted that numerous actin binding proteins exert tight control over actin filament stability and function; proteins that nucleate, stabilize, sever, or disassemble actin filaments have been well described (Pollard and Borisy, 2003). However, it is less clear how the different species of actin comprising these filaments may contribute to varied function. Higher eukaryotes express six distinct actin isoforms that are grouped according to tissue expression patterns: four "muscle" actins predominate in striated (α_{sk} and α_{ca}) and smooth (α_{sm} and γ_{sm}) muscle, while the two cytoplasmic "nonmuscle" actins (β_{cyto} and γ_{cyto}) are found in all cells (Rubenstein, 1990). While any two isoforms differ by less than 7% of their primary sequence, the nonmuscle actins remarkably differ at only four of 375 amino acids (Vandekerckhove and Weber, 1978). The fact that β_{cyto}- and γ_{cyto}-actin sequences are evolutionarily conserved between birds and mammals strongly implies significant selective pressures have maintained slight sequence differences over time.

Individual actins have been hypothesized to perform distinct functions based on their polarized distributions in a variety of cells. Numerous studies have identified subcellular sorting of β_{cyto}- and γ_{cyto}-actin mRNA in cultured cells, including myoblasts (Hill and Gunning, 1993), osteoblasts (Watanabe et al., 1998), and neurons (Bassell et al., 1998). In situ assays have also reported discrete populations of β_{cyto}- and γ_{cyto}-actin protein in gastric parietal cells (Yao et al., 1995) and cochlear hair cells (Hofer et al., 1997), the physiological relevance of which was recently highlighted with a form of human deafness mapping to mutations in the *ACTG1* locus (van Wijk E. et al., 2003; Zhu et al., 2003).

The most extreme and well-studied examples of actin sorting are found in muscle cells, where the majority of actin localizes to the sarcomeric thin filaments and interacts with myosin to generate contractile force, while a minor population of nonmuscle actin resides in the cortical cytoskeleton (Craig and Pardo, 1983; Rybakova et al., 2000; North et al., 1994). Mouse knockout models have demonstrated the physiological significance of actin sorting in muscle: conventional ablation of α_{sk}-actin (Kumar et al., 1997), α_{ca}-actin (Crawford et al., 2002), and α_{sm}-actin (Schildmeyer et al., 2000) compromised force generation in skeletal, cardiac, and vascular smooth muscle, respectively. In contrast, little is known regarding the in vivo importance of β_{cyto}- and γ_{cyto}-actin in muscle; a hypomorphic β_{cyto}-actin allele was embryonic lethal prior to muscle differentiation (Shawlot et al., 1998) and no mouse models for γ_{cyto}-actin have been reported. In cultured myoblasts, β_{cyto}- and γ_{cyto}-actin are the predominant actin species present, but upon myoblast fusion and differentiation the nonmuscle actin, mRNAs are downregulated as muscle isoform expression is turned on (McHugh et al., 1991). Transfection studies that disrupted proper nonmuscle actin regulation induced abnormal cell shapes in cultured myoblasts (Schevzov et al., 1992), myotubes (Lloyd et al., 2004), and cardiomyocytes (von Arx et al., 1995), suggesting muscle cytoskeletal architecture is heavily influenced by both β_{cyto}- and γ_{cyto}-actin. These data have contributed to a model in which γ_{cyto}-actin participates in sarcomere assembly by organizing the formation of immature z disks (Lloyd et al., 2004), leading to properly formed sarcomeres upon differentiation. In mature

*Correspondence: jervasti@umn.edu
[4] Present address: University of Minnesota, Department of Biochemistry, Molecular Biology and Biophysics, 6-155 Jackson Hall, 321 Church Street SE, Minneapolis, Minnesota 55455.

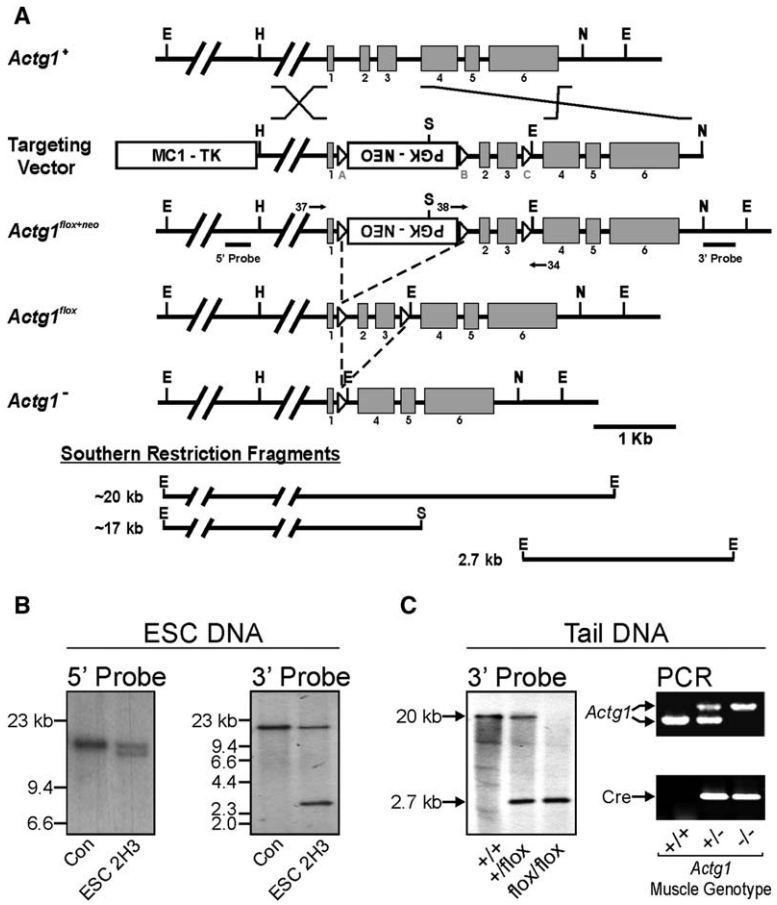

Figure 1. Generation of *Actg1*-msKO Mice

(A) Targeting scheme utilized to "flox" exons 2 and 3 of the *Actg1* allele and subsequent cre-mediated recombined alleles. Gray boxes denote exons and loxP sites are depicted as triangles. Abbreviations: EcoRI, E; HindIII, H; NcoI, N; SpeI, S.

(B) Southern blots of EcoRI/SpeI-digested ESC DNA hybridized with the appropriate probe. The wt allele yielded a ~20 kb fragment, while the targeted allele resulted in ~17 kb (5′ probe) and 2.7 kb (3′ probe) fragments.

(C) Typical genotype pattern of wt, $Actg1^{flox+neo/+}$ HSA-Cre, and $Actg1^{flox+neo/flox+neo}$ HSA-Cre (*Actg1*-msKO) mice.

skeletal muscle, γ_{cyto}-actin comprises only 1/4000 of the total actin pool (Hanft et al., 2006). However, it uniquely localizes to the costamere (Craig and Pardo, 1983; Rybakova et al., 2000), a large protein network that physically couples peripheral myofibrils to the muscle cell membrane. The costameric network is thought to radially transmit contractile force outward from the myofibrils to the extracellular matrix, adjacent muscle fibers, and beyond (Ervasti, 2003). The prevalence of disease-relevant costameric actin binding proteins suggests γ_{cyto}-actin may perform a critical role in normal muscle physiology (Ervasti, 2003). In particular, dystrophin physically couples costameric γ_{cyto}-actin filaments to the membrane (Rybakova et al., 2000) where it associates with a large transmembrane complex, termed the dystrophin glycoprotein complex (DGC). The loss of dystrophin leads to a severe form of muscular dystrophy and is characterized by costamere derangement (Williams and Bloch, 1999), increased sarcolemmal permeability, functional deficits, and muscle necrosis (Blake et al., 2002).

To explore the function of costameric γ_{cyto}-actin, we used the cre-loxP system to specifically ablate γ_{cyto}-actin expression in skeletal muscle. Although loss of γ_{cyto}-actin did not impede muscle development, muscle-specific γ_{cyto}-actin knockout (*Actg1*-msKO) mice exhibited overt symptoms of skeletal myopathy including decreased mobility, limb weakness, and joint contractures. Despite only mild costamere derangement, significant force deficits were measured both in vivo and in isolated muscles. We also observed a progressive pattern of muscle cell necrosis and regeneration that approached levels reported in dystrophin-deficient *mdx* muscle by 1 year of age. Surprisingly, the fibrosis, inflammation, and membrane damage typical of defects in the DGC were not detected. Rather, *Actg1*-msKO mice resemble a centronuclear myopathy, diseases more commonly associated with perturbations in enzyme activity, muscle development, or excitation-contraction coupling. *Actg1*-msKO mice thus support a structural basis for centronuclear myopathies and provide new opportunities to investigate the functional importance of subcellular actin isoform sorting in nonmuscle tissues.

Results

Overt Myopathy in *Actg1*-msKO Mice

β_{cyto}-actin and γ_{cyto}-actin are highly expressed and predominate in the actin-based cytoskeleton in all nonmuscle cells. To avoid the near-certain embryonic lethality of conventional γ_{cyto}-actin knockout predicted from prior studies (Shawlot et al., 1998; Harborth et al., 2001), we employed a conditional knockout approach by using the cre/loxP system.

Our targeting vector contained loxP sites flanking a neomycin cassette in intron 1 and exons 2 and 3 of the murine *Actg1* gene (Figure 1A). After electroporation into embryonic stem cells, 192 colonies surviving positive and negative selection were screened by Southern blot analysis. Probes external to both the 5′ and 3′

ends of the targeting vector identified clone 2H3 with the desired 5′ and 3′ homologous recombination events (Figure 1B). Blastocyst injections of 2H3 produced two chimeric founder mice, both of which exhibited germline transmission of the *Actg1*$^{flox+neo}$ allele.

Mice heterozygous for the neomycin cassette-containing floxed *Actg1* allele (*Actg1*$^{flox+neo/+}$) were mated with mice hemizygous for the cre transgene driven by the human α_{sk}-actin promoter (HSA-Cre; Miniou et al., 1999). The resultant mice heterozygous for *Actg1*$^{flox+neo}$ carrying the cre transgene (*Actg1*$^{flox+neo/+}$ HSA-Cre) were bred to *Actg1*$^{flox+neo/+}$ mice to generate *Actg1*$^{flox+neo/flox+neo}$ HSA-Cre (*Actg1*-msKO) mice (Figure 1C). Concurrently, heterozygous *Actg1*$^{flox+neo/+}$ mice were also crossed to mice that express cre under the control of the EIIa promoter (Holzenberger et al., 2000) to obtain partially recombined *Actg1* alleles in the germline of subsequent offspring. Heterozygous *Actg1*$^{flox/+}$ mice in which cre-mediated recombination occurred between loxP sites "A" and "B" were produced. An F_1 *Actg1*$^{flox/+}$ male was mated with a C57BL/6 female to remove the EIIa-Cre transgene from the *Actg1*^{flox} lineage. F_2 *Actg1*$^{flox/+}$ mice were bred to HSA-Cre mice as above to generate *Actg1*$^{flox/flox}$ HSA-Cre mice. *Actg1*$^{flox/flox}$ HSA-Cre and *Actg1*$^{flox+neo/flox+neo}$ HSA-Cre mice were analyzed in parallel and exhibited identical muscle phenotypes.

While Western blots of SDS-extracts from nonmuscle tissues reported normal γ_{cyto}-actin expression in *Actg1*-msKO mice (Figure 2A), Western blots of low-salt skeletal and cardiac muscle extracts enriched with DNase-I affinity chromatography (Figure 2B) established effective ablation of γ_{cyto}-actin expression in skeletal muscle only (Figure 2C and Figure S1; see the Supplemental Data available with this article online). Identical transfers probed with actin isoform-specific antibodies failed to identify a compensatory upregulation of any other actin isoform (Figure 2D). Immunohistochemistry on wt and *Actg1*-msKO tissue also confirmed a specific loss of γ_{cyto}-actin reactivity in skeletal muscle while it remained in vascular endothelium (Figure 2E).

Actg1-msKO mice were live born at expected Mendelian ratios, were viable, fertile, and showed normal growth up to 1 year of age (Figure 2F). However, *Actg1*-msKO mice were easily distinguished from littermate controls because of reduced mobility, while two-thirds of *Actg1*-msKO mice displayed classical hind limb contractures upon tail suspension (Figure 2G). The sedentary behavior and contractures persisted throughout life without noticeable worsening and did not result in premature death of *Actg1*-msKO mice.

γ_{cyto}-Actin Deficiency Causes Progressive Muscle Necrosis and Regeneration

Centrally nucleated fibers (CNFs) result from regeneration after fiber damage or necrosis and are thus a nonspecific but quantifiable index of muscle degeneration/regeneration. Although dystrophin-deficient *mdx* mice are overtly normal, *mdx* muscle undergoes repeated rounds of necrosis/regeneration beginning at 3 weeks of age, eventually plateauing at 60%–80% CNFs by 5 months of age (Blake et al., 2002). Coincident with the onset of histological abnormalities in *mdx* muscle, membrane fragility is evidenced by dramatically elevated levels of the muscle enzyme creatine kinase (CK) and uptake of the membrane impermeable dye Evans Blue (Blake et al., 2002). Despite the early clinical signs of muscle weakness in *Actg1*-msKO mice, hematoxylin and eosin (H&E) stained muscle cryosections of wt and *Actg1*-msKO muscle were indistinguishable at 1 month of age (Figure 3A). Fibers were regular in shape and appearance and peripherally nucleated in all muscles examined (Figures 3A and 3B), suggesting that muscle development proceeded normally in the absence of γ_{cyto}-actin. Furthermore, ultrastructural analysis revealed a typical striated pattern with properly assembled sarcomeres and regularly spaced z disks (Figure 3C). However, by 3 months of age, small focal areas of CNFs became evident and progressed to widespread incidence in 12 and 18 month-old *Actg1*-msKO mice (Figures 3A and 3B). In addition, fiber sizes were significantly more variable compared to controls (Figure 3D). While muscles in which type II fibers predominate were similarly affected (tibialis anterior [TA], triceps, gastrocnemius, and quadriceps), the soleus, composed primarily of type I fibers, appeared histologically normal (Figure 4A). Serial cryosections stained for either slow or fast myosin heavy chain also demonstrated type II fibers were preferentially affected (Figure 4B). Surprisingly, *Actg1*-msKO muscle displayed no evidence of membrane damage, exhibiting normal serum CK levels (Figure 4C) and little to no EBD uptake in muscle (Figure 4D). In contrast, *mdx* mice demonstrated ~8- to 10-fold higher levels of serum CK (Figure 4C) and EBD uptake in ~5%–10% of all fibers (Figure 4D). The rate and extent of regeneration in *Actg1*-msKO mice was comparable in all mice examined but was not accompanied by the inflammation and fibrosis typical of *mdx* muscle. Therefore, the progressive nature of the *Actg1*-msKO regeneration combined with the absence of fibrosis and membrane damage indicate that dystrophin and γ_{cyto}-actin deficiency cause distinct modes of cell degeneration.

While the mechanism of nuclear tethering and localization to the muscle cell periphery is not well understood, it likely involves the actin-based cytoskeleton (Starr and Han, 2003). Therefore, the central nuclei in *Actg1*-msKO muscle could be due to loss of a nuclear anchoring function. However, cryosections from 3 month old *Actg1*-msKO muscle stained with antibodies to the developmental isoform of myosin heavy chain (dMHC) revealed small pockets of dMHC-positive fibers in *Actg1*-msKO muscle (Figure 4E), strongly suggesting γ_{cyto}-actin ablation caused cell necrosis/injury and regeneration.

DGC Expression and Costamere Organization

Consistent with the lack of elevated CK levels (Figure 4C), no difference in staining patterns of DGC components was observed between wt and *Actg1*-msKO mice. All DGC members localized to the sarcolemma of both centrally and peripherally nucleated fibers (Figure 5A). In addition, immunoblot analysis of whole-muscle SDS extracts revealed normal levels of DGC expression (data not shown).

We cut longitudinal sections from perfusion-fixed muscle to definitively assess membrane cytoskeletal architecture in *Actg1*-msKO muscle. Although a regular,

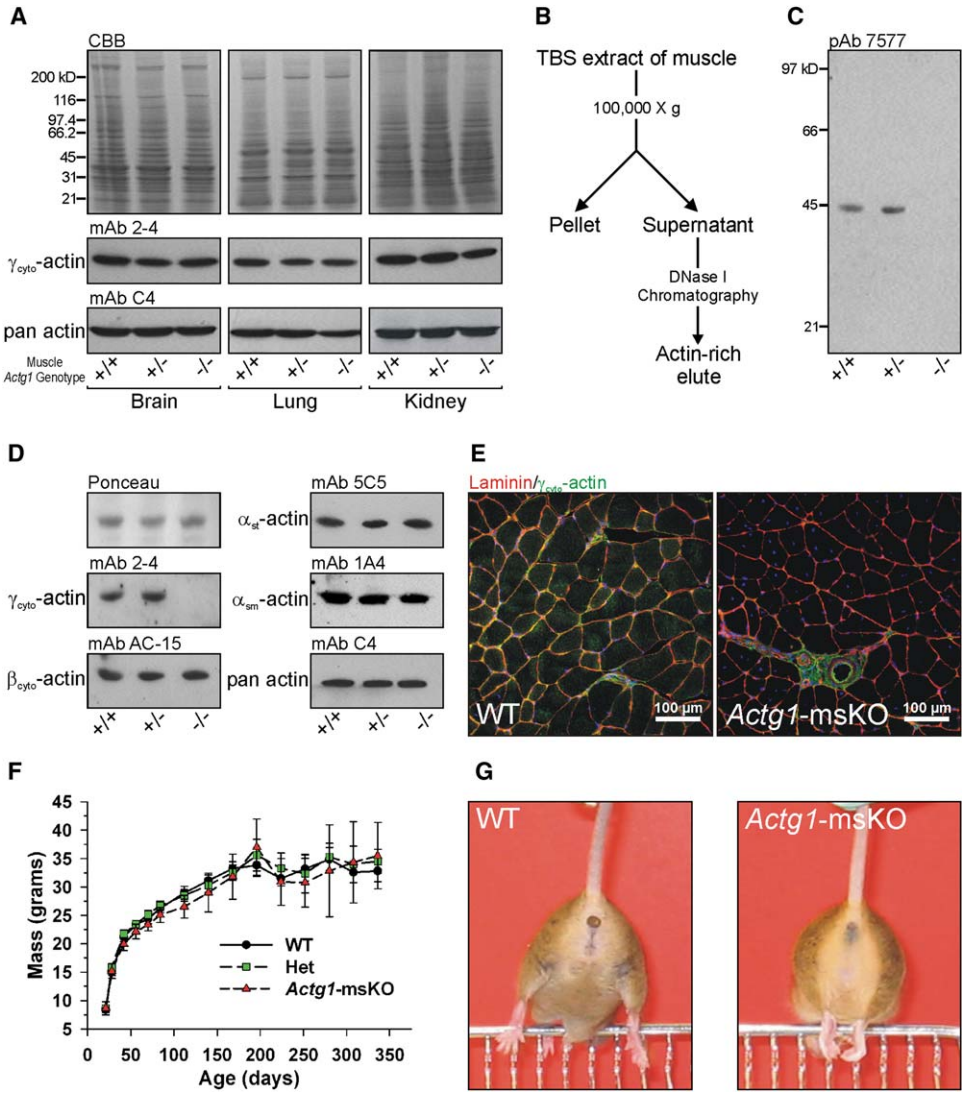

Figure 2. Muscle-Specific Ablation of γ_{cyto}-Actin Expression Results in Overt Myopathy

(A) SDS-extracts from nonmuscle tissues of wt, heterozygous, and *Actg1*-msKO mice were analyzed by SDS-PAGE and stained with Coomassie blue (CBB) or transferred to nitrocellulose. Western blots were performed with a monoclonal antibody to γ_{cyto}-actin (2–4) or pan actin antibody (C4).

(B) A TBS extraction and DNase I-affigel enrichment protocol was followed to assess expression levels of cytoplasmic actin isoforms in skeletal muscle.

(C) Western blot analysis of the actin-rich elute from (B) of wt, heterozygous, and *Actg1*-msKO skeletal muscle using γ_{cyto}-actin-specific pAb 7577.

(D) Western blots of identical nitrocellulose membranes from (C) using a panel of actin isoform-specific antibodies.

(E) Ten micron thick cryosections of wt and *Actg1*-msKO gastrocnemius muscle stained with antibodies against laminin and γ_{cyto}-actin to further demonstrate muscle specificity of γ_{cyto}-actin ablation.

(F) Growth curves of male wt, heterozygous, and *Actg1*-msKO mice up to 1 year of age. Error bars represent SEM.

(G) *Actg1*-msKO mice demonstrated reduced cage mobility and overt hind-limb contractures upon tail suspension.

striated costameric pattern was apparent in *Actg1*-msKO quadriceps and TA muscles, the pattern of dystrophin staining at the z line appeared less organized than in controls (Figure 5B). Dystrophin immunoreactivity was more broadly distributed across the z line, suggesting the loss of γ_{cyto}-actin mildly destabilized the costameric cytoskeleton. These data indicate γ_{cyto}-actin is not required for DGC expression and localization or costamere formation but is necessary for proper organization of the costameric network.

Actg1-msKO Mice Display Deficits in Force Production

To determine the functional consequences of γ_{cyto}-actin ablation, we assessed the physiologic performance of wt, *Actg1*-msKO, and *mdx* muscle both in vivo and in isolated *extensor digitorum longus* (EDL) muscles. In vivo performance was determined by measuring whole-body tension (WBT), defined as the extent of forward pulling tension exerted in response to a gentle tail pinch (Carlson and Makiejus, 1990). Although the

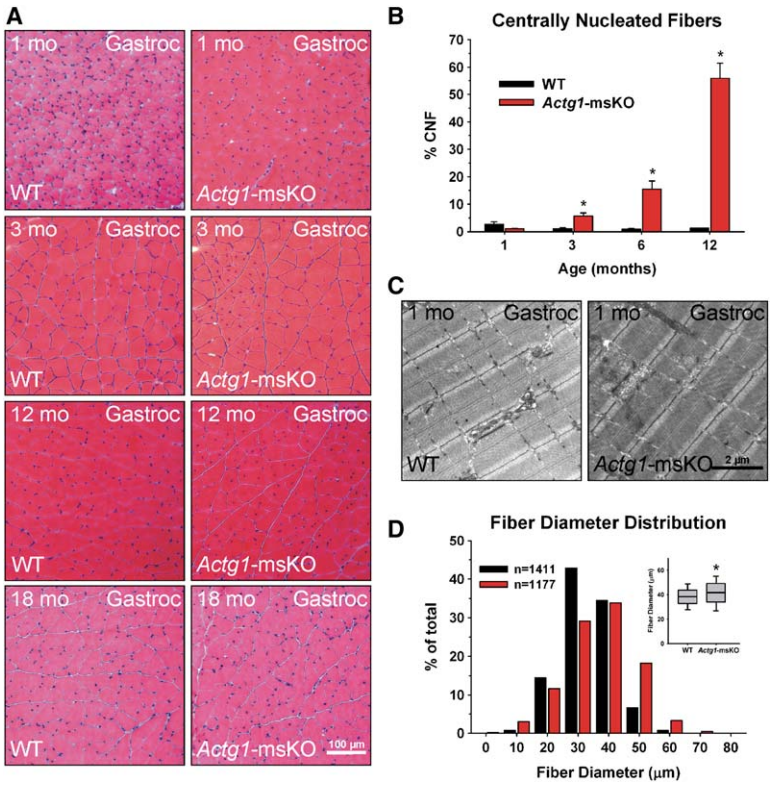

Figure 3. Progressive Necrosis and Regeneration in γ_{cyto}-Actin-Deficient Muscle

(A) H&E-stained gastrocnemius cryosections from 1, 3, 12, and 18 month old mice, respectively.

(B) Quantification of gastrocnemius CNFs from wt and *Actg1*-msKO mice ($n \geq 3$ for each genotype/time point).

(C) Electron micrographs from 1 month old wt and *Actg1*-msKO muscles to demonstrate proper sarcomere assembly.

(D) Fiber size distribution (histogram) and fiber size variability (box plot, inset) in 6 month old gastrocnemius muscles. While the average fiber diameter was similar between genotypes, the variance among *Actg1*-msKO fibers was significant (t test, $p < 0.05$). Error bars in (B) and (D) represent SEM. Unless otherwise noted, data were compared using ANOVA with Tukey post hoc test. For all figures, asterisk denotes statistical significance from wt, $p < 0.05$; pound sign denotes statistical significance from *Actg1*-msKO, $p < 0.05$.

kinetics of individual responses did not differ between the three lines of mice (Figure 6A), wt animals produced significantly greater maximal responses compared to both *Actg1*-msKO and *mdx* mice (Figure 6B). WT WBT_1 (148.9 ± 6.3 mN/g; avg ± SEM) and WBT_{1-5} (133.2 ± 3.2 mN/g) values were 28% and 24% higher

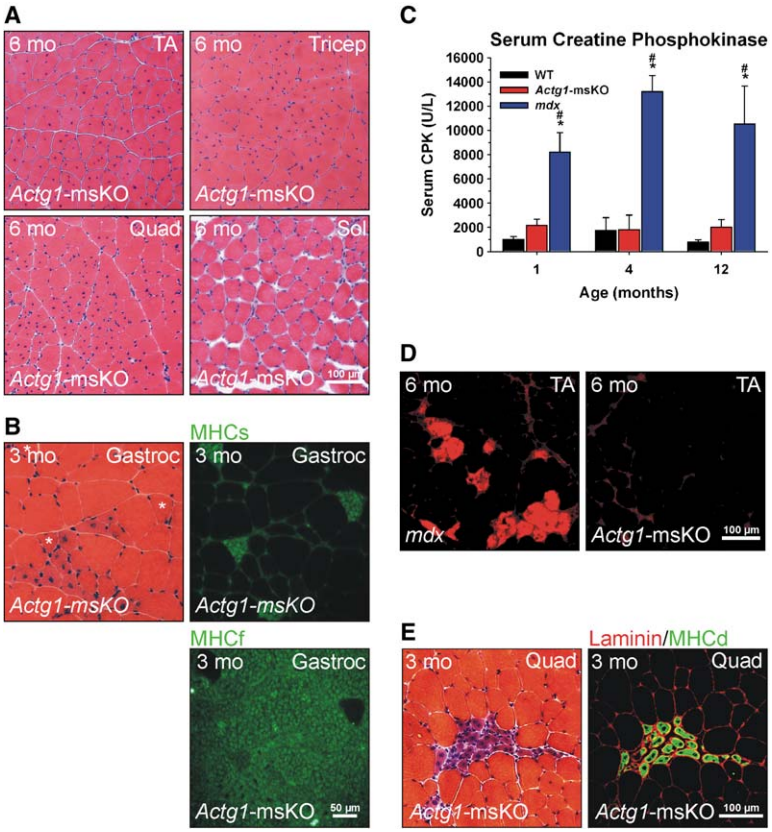

Figure 4. Lack of Membrane Damage in *Actg1*-msKO Muscle

(A) H&E-stained cryosections from 6 month old *Actg1*-msKO TA, triceps, quadriceps, and soleus.

(B) Serial H&E- and immunofluorescence-analyzed sections from *Actg1*-msKO muscle stained with 1° antibodies to slow (MHCs) and fast (MHCf) myosin heavy chains to demonstrate fiber-type specificity of muscle regeneration. Asterisk (*) denotes slow fibers in H&E-stained section.

(C) Time course analysis of serum levels of creatine phosphokinase as a marker for membrane permeability ($n \geq 4$ for each genotype at each time point). Error bars represent SEM.

(D) Cryosections of 6 month old *mdx* and *Actg1*-msKO littermate mice injected with EBD. Red-stained cells are evidence of dye uptake.

(E) Serial H&E- and immunofluorescence-analyzed sections from *Actg1*-msKO muscle stained for laminin and the developmental myosin heavy chain (MHCd) to demonstrate presence of regenerating fibers in *Actg1*-msKO muscle.

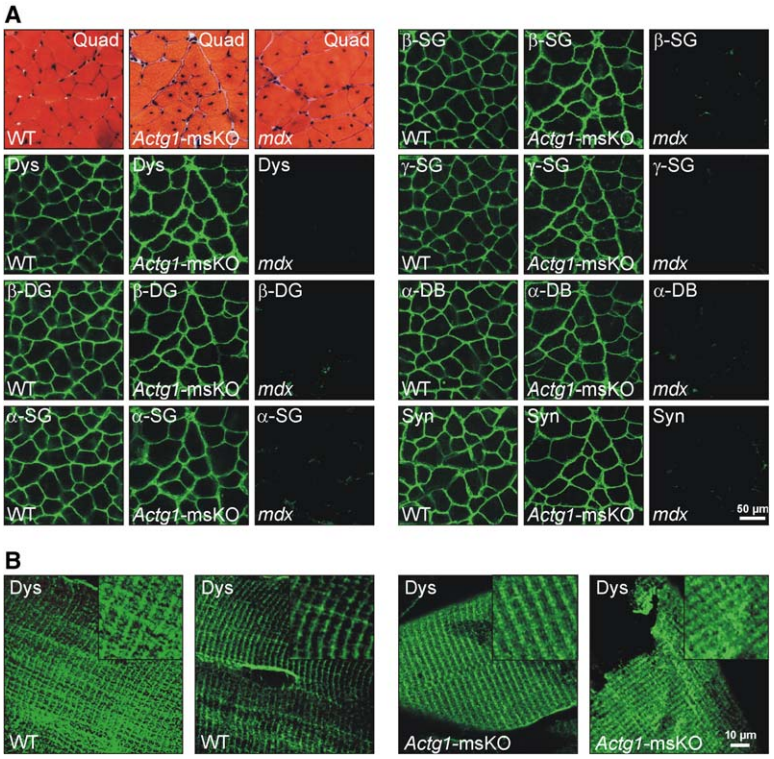

Figure 5. Localization of Dystrophin and the DGC in *Actg1*-msKO Muscle

(A) Serial cryosections from 3 month old wt, *Actg1*-msKO, and dystrophin-deficient *mdx* quadriceps muscle stained with H&E and analyzed by immunofluorescence using a 1° antibodies against assorted DGC proteins.

(B) Longitudinal cryosections from perfusion-fixed TA muscles analyzed with immunofluorescence using a 1° antibody against dystrophin.

than those for *Actg1*-msKO mice (WBT_1: 112.7 ± 11.5 mN/g; $WBT_{1–5}$: 95.6 ± 5.1 mN/g), respectively. While the force deficit observed in *Actg1*-msKO mice was less severe than that observed for *mdx* mice (WBT_1: 70.0 ± 5.1 mN/g; $WBT_{1–5}$: 61.2 ± 2.7 mN/g), only the difference in WBT_1 was significant between *Actg1*-msKO and *mdx*.

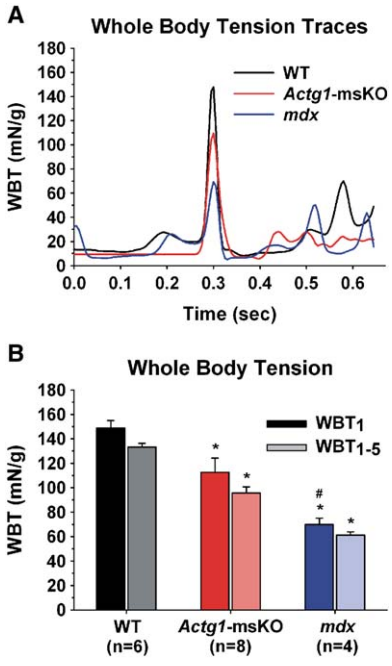

Figure 6. *Actg1*-msKO Mice Exhibit Functional Deficits In Vivo

Whole-body tension analysis in 2–3 month old mice. (A) Representative traces corresponding to single pinch responses from wt, *Actg1*-msKO, and *mdx* mice. (B) Averages of the maximal response (WBT_1) and the top five responses ($WBT_{1–5}$) from each line of mice. Error bars represent SEM.

To assess the functional decrement in single muscles, contractile properties of isolated EDL muscles were determined for wt, *Actg1*-msKO, and *mdx* mice at both 2–3 and 11–12 months of age. Despite the overt weakness exhibited by *Actg1*-msKO mice, isolated muscles demonstrated near wt levels of maximal tetanic force (Figure 7A), specific force (Figure 7B), responded normally to stretch during tetanic stimulation (eccentric contraction protocol [ECC]) (Figure 7C), and excluded Procion orange infiltration after five ECCs (data not shown). *Actg1*-msKO muscle only differed from wt in the force generated in response to a single action potential, producing 32% less twitch force than wt (Figure 7D). In contrast, *mdx* EDL muscles behaved as reported by others (Harper et al., 2002), exhibiting a significant ~20% deficit in specific force (Figure 7B). A heightened sensitivity to eccentric contractions was also observed as *mdx* muscles lost more than 80% of their force generating capacity after five ECCs at 1 year of age (Figure 7C) with a dramatic uptake of Procion orange (data not shown).

The reduction in isometric twitch force observed in *Actg1*-msKO muscle could be caused by either submaximal Ca^{2+} release in response to a single action potential or the introduction of compliance into the contractile apparatus, which would reduce the amount of force measured at the tendons. Therefore, we analyzed the Ca^{2+} transients in isolated wt and *Actg1*-msKO flexor digitorum brevis (FDB) muscle fibers in response to a single action potential. A total of 21 wt and 27 *Actg1*-msKO fibers were studied and the resultant fluorescence ratio normalized against resting [Ca^{2+}] in order

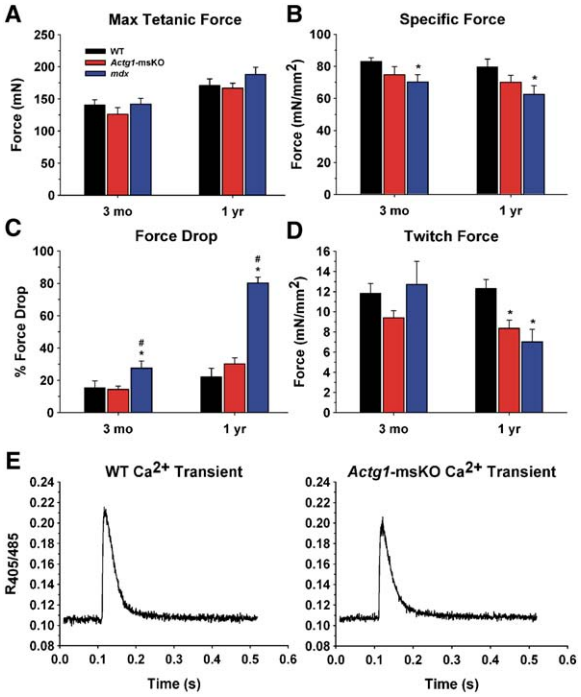

Figure 7. Contractile Properties of *Actg1*-msKO Muscle

Isometric and eccentric contraction properties of wt, *Actg1*-msKO, and *mdx* EDL muscles were assessed at 3 and 12 months of age. Tetanic force generation before (A, Max Tetanic Force) and after (B, Specific Force) normalizing against cross-sectional area of isolated EDLs. (C) Drop in tetanic force generation between ECC1 and ECC5. (D) Twitch force was lower in *Actg1*-msKO mice compared to wt controls. Error bars in (A)–(D) represent SEM. (E) Fluorescent ratios corresponding to action-potential evoked Ca^{2+} release in isolated *Actg1*-msKO and wt FDB muscles.

to directly compare experiments performed by using different light sources (Figure 7D). No differences were observed for resting or peak fluorescence ratios between wt and *Actg1*-msKO muscles (resting: 0.1058 ± 0.0021 versus 0.1069 ± 0.0027; peak: 0.2070 ± 0.0001 versus 0.1984 ± 0.0048; mean RFU ± SD for wt versus *Actg1*-msKO, respectively). Normal Ca^{2+} levels in *Actg1*-msKO muscle eliminate perturbations to the structure or function of excitation-contraction coupling proteins as the mechanism behind *Actg1*-msKO twitch force deficits but is consistent with defects in connectivity between adjacent muscle fibers and/or myofibrils or at the myotendinous junctions, causing increased compliance and reduced twitch-force generation.

Discussion

Investigations to understand the functional specificity of nonmuscle actin isoforms have traditionally focused on identifying examples of subcellular actin sorting in situ (Yao et al., 1995; Hofer et al., 1997) and transfection studies in vitro (Schevzov et al., 1992). The results of the present study demonstrate the functional significance of nonmuscle actin sorting in muscle and identify a role for γ_{cyto}-actin in maintaining muscle cell structure and function in vivo.

Actin Isoform Expression in *Actg1*-msKO Mice

The six actin isoforms are all highly related at both the genomic and amino acid level (Vandekerckhove and Weber, 1978; Erba et al., 1988). In addition, numerous highly conserved pseudogenes for the nonmuscle actins have been described (Ng et al., 1985; Peter et al., 1988), and sequence analysis initially performed to determine the relative age of several processed γ_{cyto}-actin pseudogenes instead raised the possibility that two functional γ_{cyto}-actin genes encoding identical proteins existed in the mammalian genome (Peter et al., 1988). However, Figures 1 and 2 show that targeted cre-mediated recombination at the *Actg1* locus in mice completely ablated γ_{cyto}-actin protein expression in skeletal muscle as determined by immunoblot analysis with multiple antibodies raised against unique epitopes of γ_{cyto}-actin (Hanft et al., 2006). Therefore, we conclude that γ_{cyto}-actin is functionally expressed from a single gene in mice and that *Actg1*-msKO mice were null for γ_{cyto}-actin in muscle.

The absence of detectable changes in relative expression levels for the other actin isoforms in response to γ_{cyto}-actin deficiency also raises intriguing questions regarding actin gene regulation (Figure 2). Targeted ablation of α_{sk}-actin (Kumar et al., 1997), α_{ca}-actin (Crawford et al., 2002), and α_{sm}-actin (Schildmeyer et al., 2000) resulted in a compensatory upregulation of other muscle actin isoforms. Because γ_{cyto}-actin comprises only 1/4000 of the total actin pool in muscle, we were not surprised by a lack of detectable upregulation of muscle actins in *Actg1*-msKO muscle as the relative degree of potential upregulation should be below detection. However, the observation that β_{cyto}-actin expression was unchanged in the absence of γ_{cyto}-actin was unexpected. Like γ_{cyto}-actin, β_{cyto}-actin is expressed at low levels in mature skeletal muscle (McHugh et al., 1991) and any relative change in expression should be detectable by Western blot. Additionally, the nonmuscle actins are thought to participate in a regulatory feedback loop to maintain proper protein levels (Lloyd et al., 1992), and pharmacological disruption of nonmuscle actin filaments has been shown to result in an upregulation of nonmuscle actin mRNA in cultured myoblasts (Lloyd et al., 1992). The results in Figure 2 indicate the mechanisms regulating nonmuscle actin expression in vivo are distinct from those in vitro.

γ_{cyto}-Actin Is Not Required for Sarcomere Assembly but Leads to a Progressive Myopathy

Actg1-msKO muscle appeared normal at 4 weeks of age (Figures 3A and 3B) and demonstrated a normal array of sarcomeric thick and thin filaments (Figure 3C), which disputes a role for γ_{cyto}-actin in myofibrillogenesis as suggested by others (Lloyd et al., 2004). Because the HSA-Cre mouse line used in this study expresses cre at the earliest stages of muscle differentiation (Miniou et al., 1999), it is unlikely that residual γ_{cyto}-actin persists throughout myogenesis to allow for proper structural development. It is possible that sufficient β_{cyto}-actin was present during early stages of muscle development to provide the scaffolding function ascribed to γ_{cyto}-actin (Lloyd et al., 2004). Therefore, it could be argued that β_{cyto}- and γ_{cyto}-actin are redundant during embryonic muscle development but their slight differences do

manifest distinct functions in mature skeletal muscle. Future analyses into the embryonic requirements for β_{cyto}- and γ_{cyto}-actin will be necessary to further explore such possibilities.

Because numerous disease-relevant actin binding proteins localize to the costamere (Ervasti, 2003), we hypothesized γ_{cyto}-actin ablation would result in a severe muscular dystrophy. Our early observations that 3 week old *Actg1*-msKO mice appeared more sedentary than wt littermates and displayed hind limb contractures (Figure 2) were consistent with those expected from a complete disruption of the DGC-actin link, as mice that lack both dystrophin and the dystrophin autosomal homolog utrophin exhibit a severe overt phenotype with contractures and premature death (Grady et al., 1997; Deconinck et al., 1997). However, in contrast to *mdx/utrn*$^{-/-}$ mice, *Actg1*-msKO mice did not die prematurely, indicating γ_{cyto}-actin ablation caused a distinct molecular phenotype compared to mice lacking dystrophin and utrophin. In addition, although initial signs of necrosis and regeneration arose at 3 months of age and proceeded to levels approaching those described for *mdx* mice at 1 year of age (Figures 3A and 3B), the complete lack of membrane fragility in the absence of γ_{cyto}-actin further distinguished *Actg1*-msKO mice from other mouse models with perturbations in the DGC, which all display similar patterns of cell death and membrane permeability at an early age. Instead, γ_{cyto}-actin deficiency resulted in a fundamental flaw in muscle structure or function that leads to a deliberate, chronic buildup of necrosis resembling the histological features ascribed to a class of human muscle diseases termed centronuclear myopathies (CNMs). The various CNMs share a similar generalized muscle weakness and are clinically diagnosed by the presence of a high proportion of skeletal muscle fibers containing central nuclei (Pierson et al., 2005). Although the underlying mechanisms of muscle weakness are unclear, defects in muscle development (Nakagawa et al., 2005) and/or structural maintenance (Buj-Bello et al., 2002) have been proposed. Interestingly, the two genes currently known to cause human CNM, the phosphatase myotubularin-encoding *MTM1* (Laporte et al., 1996) and the dynamin-2-encoding *DNM2* (Bitoun et al., 2005), have both been speculated to play roles in membrane trafficking (Bitoun et al., 2005), processes dependent on actin-based structures. In addition, *MTM1*-null mice develop a severe overt myopathy with grasping defects, kyphosis, and premature death (Buj-Bello et al., 2002). The important role of the actin cytoskeleton in membrane trafficking as well as the similar overt and histological phenotypes between *MTM1*-null mice and *Actg1*-msKO mice suggests *Actg1*-msKO mice will be useful in elucidating the pathophysiology of CNMs.

Structural Defects in γ_{cyto}-Actin-Deficient Muscle

To better understand the structural consequences leading to progressive muscle cell necrosis, we assessed the costameric lattice by immunofluorescence analysis. We (Ervasti, 2003) and others (Craig and Pardo, 1983) have hypothesized that γ_{cyto}-actin plays a fundamental role in organizing the costamere, particularly due to the numerous disease-relevant actin binding proteins that localize to the network (Ervasti, 2003). In addition, altered costameric arrays have been described in muscle lacking various DGC components (Williams and Bloch, 1999; Yurchenco et al., 2004), suggesting the interaction between the DGC and γ_{cyto}-actin is necessary for costameric stability. Besides the γ_{cyto}-actin-based cytoskeleton, intermediate filament (IF) proteins have also been speculated to play a role in costamere formation, and desmin-null muscle exhibited dramatic costameric disarray in several different muscle groups (O'Neill et al., 2002). However, some muscles possessed normal costameric patterns (O'Neill et al., 2002) and Shah et al. concluded that desmin was not essential for the costameric connection of peripheral myofibrils and the sarcolemma (Shah et al., 2004). Therefore, we were surprised at the relatively mild disorganization of costameres in γ_{cyto}-actin deficient muscle (Figure 5B). These data suggest that the factors involved in costamere organization may be muscle-type specific and that more than one type of cytoskeletal element is required.

Force Deficits in γ_{cyto}-Actin-Deficient Muscle Are Consistent with Defects in Fiber and/or Fibril Attachments

The combined results in Figures 6 and 7 verify the essential nature of γ_{cyto}-actin in normal muscle physiology. We speculate that the observed functional deficit in isometric twitch force (Figure 7A) in the presence of normal action potential-evoked Ca^{2+} release (Figure 7E) results from defects in either attachments between myofibrils within a cell, between individual muscle cells themselves, or at the myotendinous junction. A decreased efficiency of force production due to decreased lateral stiffness is not without precedent. Distinct from its disputed role at the costamere, it is well accepted that desmin plays an essential role connecting individual myofibrils at the z disk (Paulin and Li, 2004). Desmin-deficient muscle consequently generates less maximal isometric force and exhibits decreased lateral stiffness and misalignment between adjacent muscle fibers (Paulin and Li, 2004). Future studies are thus necessary to better understand the relationship between loss of γ_{cyto}-actin and the observed consequences for force generation.

Conclusions

Our results demonstrate the in vivo importance of subcellular γ_{cyto}-actin sorting in striated muscle. Future studies aimed at measuring the lateral stiffness of γ_{cyto}-actin deficient muscle promise to help elucidate the structural perturbations leading to the observed force deficits and provide new insight into the role of the costameric cytoskeleton in diseases of striated muscle. *Actg1*-msKO mice also present a potential mouse model for the genetically undefined centronuclear myopathies and support the screening of genetically undiagnosed patients for mutations in the *ACTG1* allele. Finally, the floxed *Actg1* allele provides a unique and invaluable tool to better understand the role of γ_{cyto}-actin and subcellular actin sorting in nonmuscle cells.

Experimental Procedures

Construction of Targeting Vector and Generation of *Actg1*-msKO Mice

A 12 kb mouse genomic clone pMgCGA-15D (provided by Dr. James Lessard, University of Cincinnati) encoding the γ_{cyto}-actin locus

(*Actg1*) was used to assemble the floxed *Actg1* construct pKO-ScAB. A full description of pKO-ScAB construction is available in the Supplemental Data.

pKO-ScAB was linearized and electroporated into R1 murine embryonic stem cells. Colonies surviving selection were isolated, expanded, and screened by Southern blot analysis (see Supplemental Data for details). Clone 2H3 was identified with the expected 5′ and 3′ recombination events and was subsequently karyotyped and injected into C57BL/6 blastocysts. Chimeric males were bred to C57BL/6 females to determine germline transmission of the floxed allele. Agouti offspring heterozygous for the floxed *Actg1* allele (*Actg1*$^{flox+neo/+}$) were bred with transgenic mice that express cre recombinase under the control of the human α_{sk}-actin promoter (HSA-Cre mice were provided by Dr. Judith Melki, INSERM, France) (Miniou et al., 1999). Heterozygous *Actg1*$^{flox+neo/+}$ hemizygous cre mice were then bred to *Actg1*$^{flox+neo/+}$ mice to obtain homozygous floxed mice carrying the cre transgene (*Actg1*$^{flox+neo/flox+neo}$HSA-Cre).

Actg1$^{flox+neo/+}$ mice were also bred with mice that express cre under the control of the germline-expressed EIIa promoter (Holzenberger et al., 2000) in order to selectively remove the neomycin cassette from the floxed allele in the germline. F_1 males were mated with C57BL/6 females to screen for partial recombination between loxP sites "A" and "B." Subsequent *Actg1*$^{flox/+}$ mice were backcrossed two generations to C57BL/6 mice and then bred to homozygosity with HSA-Cre as above. Both *Actg1*$^{flox+neo/flox+neo}$ HSA-Cre and *Actg1*$^{flox/flox}$ HSA-Cre mice were analyzed in parallel and exhibited an identical muscle phenotype. Therefore, data from both lines were pooled for subsequent analyses.

All genotype analyses of the *Actg1* locus were performed by Southern blot or a multiplex PCR (see Supplemental Data for primer descriptions). Cre genotypes were determined as described (Miniou et al., 1999). Animals were housed and treated in accordance with the standards set by the University of Wisconsin Institutional Animal Care and Use Committee.

Antibodies

Polyclonal (7577) and monoclonal antibodies to γ_{cyto}-actin (2–4) were described previously (Hanft et al., 2006). Anti-dystrophin Rb2 was also described elsewhere (Rybakova et al., 2000). Pan-actin antibody (C4) was the kind gift of Dr. James Lessard. Polyclonal anti-laminin and monoclonal antibodies to vinculin (hVIN-1), striated α-actin (5C5), β_{cyto}-actin (AC15), and α_{sm}-actin (1A4) were purchased from Sigma. Antibodies to dystrophin (Dys3), β-dystroglycan (b-DG), α-sarcoglycan (a-SARC), β-sarcoglycan (b-SARC), γ-sarcoglycan (g-SARC), developmental myosin heavy chain (dMHC), and slow/fast myosin heavy chain (MHCs/MHCf) were purchased from Novacastra. Peroxidase-conjugated anti-rabbit and anti-mouse secondary antibodies were purchased from Bio-Rad and Roche, respectively.

Protein Extracts and Western Blot Analysis

Mice were anesthetized with avertin and killed by cervical dislocation. Tissues were quickly dissected and snap frozen in liquid N_2. SDS-extracts of nonmuscle tissues were performed as described (Hanft et al., 2006). Twenty-five micrograms of protein/sample was separated by SDS-PAGE and transferred to nitrocellulose. Analysis of actin isoform expression in muscle followed a low-salt extraction and DNase-I amplification protocol as described (Hanft et al., 2006).

Histology and Morphometric Analysis

Individual muscles were dissected, coated with OCT (TissueTek), and rapidly frozen in liquid N_2-cooled isopentane. Ten micron thick cryosections were cut on a Leica CM3050 cryostat, air dried, and stained with hematoxylin and eosin-phloxine as described (Harper et al., 2002). Sections cut from the muscle midbelly were selected for analysis. Images were collected on a Zeiss Axiovert 25 microscope and compiled into montages of entire sections in CorelDraw 10 and exported to Scion Image for morphometric analyses. The percentage of CNFs was determined by scoring every muscle fiber in one gastrocnemius muscle from 1, 3, 6, and 12 month old mice ($n \geq 3$ for each genotype at each time point). Fiber-size variability was determined in 6 month old mice as described (Harper et al., 2002) from the same muscle used for CNF analysis. Student's t tests were performed to compare average CNF values at each time point and average fiber diameter. Significance of fiber diameter variability was determined by a Student's t test on the standard deviations of individual muscle sections (Harper et al., 2002). One percent EBD in PBS was injected intraperitoneally into 6 month old *Actg1*-msKO and *mdx* mice. Sixteen hours postinjection, mice were killed and analyzed. Serial cryosections were analyzed by H&E, and images of EBD positive fibers were collected on a Zeiss Axiovert 25 microscope equipped for epifluorescence and exported to CorelDraw 10 for figure preparation. Serum creatine kinase levels were determined with Vitros CK DT slides (Ortho-Clinical Diagnostics) and measured with a Kodak Ektachem DT60 Analyzer. Data were collected in units/ml.

Immunohistochemistry

Ten micron thick transverse cryosections were fixed in 4% paraformaldehyde for 10 min, washed in phosphate-buffered saline (PBS), and blocked in 5% goat serum for 30 min. Sections were incubated with 1° antibodies in 5% goat serum overnight at 4°C and washed in PBS. Alexa-488- or 568-conjugated 2° antibodies (Molecular Probes) were incubated for 30 min before a final PBS wash cycle. Coverslips were applied with a drop of Anti-Fade Reagent (Molecular Probes) and confocal images obtained with a Bio-Rad MRC1000 scan head mounted transversely to an inverted Nikon Diaphot 200 microscope at the Keck Center for Biological Imaging. Images from each mouse model were obtained under identical laser and optical conditions for each antibody and exported to CorelDraw 10 for figure preparation.

Costamere imaging was performed as described (Williams and Bloch, 1999). Confocal images from wt and *Actg1*-msKO muscle were obtained as above and exported to Scion Image for analysis.

Electron Microscopy

Anesthetized mice were transcardially perfusion-fixed with 2% gluteraldehyde. Skeletal muscle was processed for EM by postfixation with 2% osmium tetroxide in PBS for 1 hr, washed in PBS, and dehydrated in ethanol. Dehydrated tissues were embedded in Embed-812 (Electron Microscopy Sciences), sectioned at 60 nm, and stained with 5% uranyl acetate and 1% lead citrate. Sections were viewed and photographed on a Jeol 100CX transmission electron microscope.

Whole-Body Tension

The "escape" test protocol was adapted from Carlson and Makiejus (1990) with slight modifications. Ten to 12 week old wt, *Actg1*-msKO, and *mdx* mice ($n \geq 4$ for each genotype) were placed between parallel wooden barriers to allow for forward movement only. Silk suture was used to attach the mouse tail to a fixed range force transducer (BioPac Systems) to record the force evoked by a light tail pinch. Five minute traces with ~5 pinches/min were collected and the evoked peaks measured and normalized against mouse body mass. Data were analyzed in two ways: WBT_1, magnitude of maximum peak observed for each mouse; WBT_{1-5}, average of top five peaks observed for each mouse.

Maximal Force and Eccentric Contractions

All mechanical properties were modeled after (Petrof et al., 1993). Two to 3 month or 11 to 12 month old sex-matched *Actg1*-msKO mice, littermate controls, and *mdx* mice ($n \geq 5$ for each genotype at each time point) were sacrificed and the EDL muscles dissected. 4/0 silk suture was used to attach the proximal tendon to a rigid support and the distal tendon to a servomotor (Model 300B-LR, Aurora Scientific) in an organ bath filled with a Ca^{2+}-Ringer's solution (in mM: 120.5 NaCl, 4.8 KCl, 1.2 $MgSO_4$, 1.2 Na_2HPO_4, 20.4 $NaHCO_3$, 10 glucose, 10 pyruvate, and 1.5 $CaCl_2$ [pH 7.6]) and allowed to equilibrate. The solution was continuously gassed with 95% O_2/5% CO_2 to maintain a pH of 7.6 at 30°C. Muscles were stimulated with a single pulse (200 μs in duration) with two platinum plate electrodes on either side of the muscle. Muscle lengths were progressively lengthened to an optimal length (L_o) that elicited maximal twitch tension.

Protection against mechanical injury was assessed by subjecting each muscle to an ECC protocol, which consisted of five maximal tetanic stimulations (150 Hz for 700 ms duration). Each ECC involved tetanic stimulation for 700 ms, with a stretch of 0.5 L_o/s over the final 200 ms to result in a total stretch of 0.1 L_o. Five minutes of recovery time was allowed between each measurement. Force drop was calculated as ([ECC1 − ECC5]/ECC1). After analysis, each muscle was

bathed in 0.1% Procion orange, washed, and frozen for cryosectioning. Dye uptake was quantified by counting the dye-positive fibers.

Calcium Transients

Single muscle fibers were enzymatically dissociated from FDB muscles of 5 to 6 week old wt and *Actg1*-msKO littermate mice and cultured on laminin coated glass coverslips as described previously (Liu et al., 1997). Cultures were loaded with 1 μM Indo-1AM in DMSO, rinsed with Ringer's solution, and equilibrated before recording. The culture chamber was mounted on an Olympus IX71 inverted microscope and viewed with an Olympus 60×/1.20 NA water immersion objective. Fibers were illuminated at 360 nm, and the fluorescence emitted at 405 nm and 485 nm was detected simultaneously. The emission signal was filtered at 2 kHz, digitized, and sampled repetitively at 500 μs intervals with the use of a data-collection program (Patchmaster, Heka), and the fluorescence ratio F_{405}/F_{485} calculated. Two platinum electrodes connected were used to stimulate fibers with a single pulse (1 ms duration). The stimulation voltage was adjusted to give observed fiber contraction in all cases. Most fibers remained attached to the coverslip throughout the period of stimulation and recovery, and only these fibers were used to obtain the data reported.

Statistical Analysis

All data were presented as means ± SEM. Unless otherwise noted, comparisons between groups were performed by ANOVA followed by a Tukey post hoc test to determine significance at $p < 0.05$.

Supplemental Data

Supplemental Data including Supplemental Experimental Procedures and one Supplemental Figure are available at http://www.developmentalcell.com/cgi/content/full/11/3/■■■/DC1/.

Acknowledgments

The authors thank Michele Jaeger and Kurt Prins for technical assistance and Drs. James Lessard and Judith Melki for reagents and mice, respectively. This work was supported by an American Heart Association Pre-Doctoral Fellowship and grants from the Muscular Dystrophy Association, the National Institutes of Health (AR049899), and National Research Service Award T32 HL07936 from the University of Wisconsin-Madison Cardiovascular Research Center.

Received: March 9, 2006
Revised: June 21, 2006
Accepted: July 6, 2006
Published: September 1, 2006

References

Bassell, G.J., Zhang, H., Byrd, A.L., Femino, A.M., Singer, R.H., Taneja, K.L., Lifshitz, L.M., Herman, I.M., and Kosik, K.S. (1998). Sorting of β-actin mRNA and protein to neurites and growth cones in culture. J. Neurosci. *18*, 251–265.

Bitoun, M., Maugenre, S., Jeannet, P.Y., Lacene, E., Ferrer, X., Laforet, P., Martin, J.J., Laporte, J., Lochmuller, H., Beggs, A.H., et al. (2005). Mutations in dynamin 2 cause dominant centronuclear myopathy. Nat. Genet. *37*, 1207–1209.

Blake, D.J., Weir, A., Newey, S.E., and Davies, K.E. (2002). Function and genetics of dystrophin and dystrophin-related proteins in muscle. Physiol. Rev. *82*, 291–329.

Buj-Bello, A., Laugel, V., Messaddeq, N., Zahreddine, H., Laporte, J., Pellissier, J.F., and Mandel, J.L. (2002). The lipid phosphatase myotubularin is essential for skeletal muscle maintenance but not for myogenesis in mice. Proc. Natl. Acad. Sci. USA *99*, 15060–15065.

Carlson, C.G., and Makiejus, R.V. (1990). A noninvasive procedure to detect muscle weakness in the mdx mouse. Muscle Nerve *13*, 480–484.

Craig, S.W., and Pardo, J.V. (1983). Gamma actin, spectrin, and intermediate filament proteins colocalize with vinculin at costameres, myofibril-to-sarcolemma attachment sites. Cell Motil. *3*, 449–462.

Crawford, K., Flick, R., Close, L., Shelly, D., Paul, R., Bove, K., Kumar, A., and Lessard, J. (2002). Mice lacking skeletal muscle actin show reduced muscle strength and growth deficits and die during the neonatal period. Mol. Cell. Biol. *22*, 5887–5896.

Deconinck, A.E., Rafael, J.A., Skinner, J.A., Brown, S.C., Potter, A.C., Metzinger, L., Watt, D.J., Dickson, J.G., Tinsley, J.M., and Davies, K.E. (1997). Utrophin-dystrophin-deficient mice as a model for Duchenne muscular dystrophy. Cell *90*, 717–727.

Erba, H.P., Eddy, R., Shows, T., Kedes, L., and Gunning, P. (1988). Structure, chromosome location, and expression of the human γ-actin gene: differential evolution, location, and expression of the cytoskeletal β- and γ-actin genes. Mol. Cell. Biol. *8*, 1775–1789.

Ervasti, J.M. (2003). Costameres: the Achilles' heel of Herculean muscle. J. Biol. Chem. *278*, 13591–13594.

Grady, R.M., Teng, H.B., Nichol, M.C., Cunningham, J.C., Wilkinson, R.S., and Sanes, J.R. (1997). Skeletal and cardiac myopathies in mice lacking utrophin and dystrophin: a model for Duchenne muscular dystrophy. Cell *90*, 729–738.

Hanft, L.M., Rybakova, I.N., Patel, J.R., Rafael-Fortney, J.A., and Ervasti, J.M. (2006). Cytoplasmic γ-actin contributes to a compensatory remodeling response in dystrophin-deficient muscle. Proc. Natl. Acad. Sci. USA *103*, 5385–5390.

Harborth, J., Elbashir, S.M., Bechert, K., Tuschl, T., and Weber, K. (2001). Identification of essential genes in cultured mammalian cells using small interfering RNAs. J. Cell Sci. *114*, 4557–4565.

Harper, S.Q., Hauser, M.A., DelloRusso, C., Duan, D., Crawford, R.W., Phelps, S.F., Harper, H.A., Robinson, A.S., Engelhardt, J.F., Brooks, S.V., and Chamberlain, J.S. (2002). Modular flexibility of dystrophin: implications for gene therapy of Duchenne muscular dystrophy. Nat. Med. *8*, 253–261.

Hill, M.A., and Gunning, P. (1993). Beta and gamma actin mRNAs are differentially located within myoblasts. J. Cell Biol. *122*, 825–832.

Hofer, D., Ness, W., and Drenckhahn, D. (1997). Sorting of actin isoforms in chicken auditory hair cells. J. Cell Sci. *110*, 765–770.

Holzenberger, M., Lenzner, C., Leneuve, P., Zaoui, R., Hamard, G., Vaulont, S., and Bouc, Y.L. (2000). Cre-mediated germline mosaicism: a method allowing rapid generation of several alleles of a target gene. Nucleic Acids Res. *28*, E92.

Kumar, A., Crawford, K., Close, L., Madison, M., Lorenz, J., Doetschman, T., Pawlowski, S., Duffy, J., Neumann, J., Robbins, J., et al. (1997). Rescue of cardiac α-actin-deficient mice by enteric smooth muscle γ-actin. Proc. Natl. Acad. Sci. USA *94*, 4406–4411.

Laporte, J., Hu, L.J., Kretz, C., Mandel, J.L., Kioschis, P., Coy, J.F., Klauck, S.M., Poustka, A., and Dahl, N. (1996). A gene mutated in X-linked myotubular myopathy defines a new putative tyrosine phosphatase family conserved in yeast. Nat. Genet. *13*, 175–182.

Liu, Y., Carroll, S.L., Klein, M.G., and Schneider, M.F. (1997). Calcium transients and calcium homeostasis in adult mouse fast-twitch skeletal muscle fibers in culture. Am. J. Physiol. *272*, C1919–C1927.

Lloyd, C., Schevzov, G., and Gunning, P. (1992). Transfection of non-muscle β- and γ-actin genes into myoblasts elicits different feedback regulatory responses from endogenous actin genes. J. Cell Biol. *117*, 787–797.

Lloyd, C.M., Berendse, M., Lloyd, D.G., Schevzov, G., and Grounds, M.D. (2004). A novel role for non-muscle γ-actin in skeletal muscle sarcomere assembly. Exp. Cell Res. *297*, 82–96.

McHugh, K.M., Crawford, K., and Lessard, J.L. (1991). A comprehensive analysis of the developmental and tissue-specific expression of the isoactin multigene family in the rat. Dev. Biol. *148*, 442–458.

Miniou, P., Tiziano, D., Frugier, T., Roblot, N., Le Meur, M., and Melki, J. (1999). Gene targeting restricted to mouse striated muscle lineage. Nucleic Acids Res. *27*, e27.

Nakagawa, O., Arnold, M., Nakagawa, M., Hamada, H., Shelton, J.M., Kusano, H., Harris, T.M., Childs, G., Campbell, K.P., Richardson, J.A., et al. (2005). Centronuclear myopathy in mice lacking a novel muscle-specific protein kinase transcriptionally regulated by MEF2. Genes Dev. *19*, 2066–2077.

Ng, S.Y., Gunning, P., Eddy, R., Ponte, P., Leavitt, J., Shows, T., and Kedes, L. (1985). Evolution of the functional human β-actin gene and its multi-pseudogene family: conservation of noncoding regions

and chromosomal dispersion of pseudogenes. Mol. Cell. Biol. *5*, 2720–2732.

North, A.J., Gimona, M., Lando, Z., and Small, J.V. (1994). Actin isoform compartments in chicken gizzard smooth muscle cells. J. Cell Sci. *107*, 445–455.

O'Neill, A., Williams, M.W., Resneck, W.G., Milner, D.J., Capetanaki, Y., and Bloch, R.J. (2002). Sarcolemmal organization in skeletal muscle lacking desmin: evidence for cytokeratins associated with the membrane skeleton at costameres. Mol. Biol. Cell *13*, 2347–2359.

Paulin, D., and Li, Z. (2004). Desmin: a major intermediate filament protein essential for the structural integrity and function of muscle. Exp. Cell Res. *301*, 1–7.

Peter, B., Man, Y.M., Begg, C.E., Gall, I., and Leader, D.P. (1988). Mouse cytoskeletal γ-actin: analysis and implications of the structure of cloned cDNA and processed pseudogenes. J. Mol. Biol. *203*, 665–675.

Petrof, B.J., Shrager, J.B., Stedman, H.H., Kelly, A.M., and Sweeney, H.L. (1993). Dystrophin protects the sarcolemma from stresses developed during muscle contraction. Proc. Natl. Acad. Sci. USA *90*, 3710–3714.

Pierson, C.R., Tomczak, K., Agrawal, P., Moghadaszadeh, B., and Beggs, A.H. (2005). X-linked myotubular and centronuclear myopathies. J. Neuropathol. Exp. Neurol. *64*, 555–564.

Pollard, T.D., and Borisy, G.G. (2003). Cellular motility driven by assembly and disassembly of actin filaments. Cell *112*, 453–465.

Rubenstein, P.A. (1990). The functional importance of multiple actin isoforms. Bioessays *12*, 309–315.

Rybakova, I.N., Patel, J.R., and Ervasti, J.M. (2000). The dystrophin complex forms a mechanically strong link between the sarcolemma and costameric actin. J. Cell Biol. *150*, 1209–1214.

Schevzov, G., Lloyd, C., and Gunning, P. (1992). High level expression of transfected β- and γ-actin genes differentially impacts on myoblast cytoarchitecture. J. Cell Biol. *117*, 775–785.

Schildmeyer, L.A., Braun, R., Taffet, G., Debiasi, M., Burns, A.E., Bradley, A., and Schwartz, R.J. (2000). Impaired vascular contractility and blood pressure homeostasis in the smooth muscle α-actin null mouse. FASEB J. *14*, 2213–2220.

Shah, S.B., Davis, J., Weisleder, N., Kostavassili, I., McCulloch, A.D., Ralston, E., Capetanaki, Y., and Lieber, R.L. (2004). Structural and functional roles of desmin in mouse skeletal muscle during passive deformation. Biophys. J. *86*, 2993–3008.

Shawlot, W., Deng, J.M., Fohn, L.E., and Behringer, R.R. (1998). Restricted β-galactosidase expression of a hygromycin-*lac*Z gene targeted to the β-actin locus and embryonic lethality of β-actin mutant mice. Transgenic Res. *7*, 95–103.

Starr, D.A., and Han, M. (2003). ANChors away: an actin based mechanism of nuclear positioning. J. Cell Sci. *116*, 211–216.

van Wijk, E., Krieger, E., Kemperman, M.H., De Leenheer, E.M., Huygen, P.L., Cremers, C.W., Cremers, F.P., and Kremer, H. (2003). A mutation in the gamma actin 1 (ACTG1) gene causes autosomal dominant hearing loss (DFNA20/26). J. Med. Genet. *40*, 879–884.

Vandekerckhove, J., and Weber, K. (1978). Mammalian cytoplasmic actins are the products of at least two genes and differ in primary structure in a least 25 identified positions from skeletal muscle actins. Proc. Natl. Acad. Sci. USA *75*, 1106–1110.

von Arx, P., Bantle, S., Soldati, T., and Perriard, J.C. (1995). Dominant negative effect of cytoplasmic actin isoproteins on cardiomyocyte cytoarchitecture and function. J. Cell Biol. *131*, 1759–1773.

Watanabe, H., Kislauskis, E.H., MacKay, C.A., Mason-Savas, A., and Marks, S.C., Jr. (1998). Actin mRNA isoforms are differentially sorted in normal osteoblasts and sorting is altered in osteoblasts from a skeletal mutation in the rat. J. Cell Sci. *111*, 1287–1292.

Williams, M.W., and Bloch, R.J. (1999). Extensive but coordinated reorganization of the membrane skeleton in myofibers of dystrophic (*mdx)* mice. J. Cell Biol. *144*, 1259–1270.

Yao, X., Chaponnier, C., Gabbiani, G., and Forte, J.G. (1995). Polarized distribution of actin isoforms in gastric parietal cells. Mol. Biol. Cell *6*, 541–557.

Yurchenco, P.D., Cheng, Y.S., Campbell, K., and Li, S. (2004). Loss of basement membrane, receptor and cytoskeletal lattices in a laminin-deficient muscular dystrophy. J. Cell Sci. *117*, 735–742.

Zhu, M., Yang, T., Wei, S., DeWan, A.T., Morell, R.J., Elfenbein, J.L., Fisher, R.A., Leal, S.M., Smith, R.J., and Friderici, K.H. (2003). Mutations in the γ-actin gene (ACTG1) are associated with dominant progressive deafness (DFNA20/26). Am. J. Hum. Genet. *73*, 1082–1091.